P H Y S I C A L   R E V I E W   L E T T E R S

Solid Superheating Observed in Two-Dimensional Strongly Coupled Dusty Plasma

Yan Feng,* J. Goree, and Bin Liu

Department of Physics and Astronomy, The University of Iowa, Iowa City, Iowa 52242, USA
(Received 3 April 2008; published 23 May 2008)

It is demonstrated experimentally that strongly coupled plasma exhibits solid superheating. A 2D suspension of microspheres in dusty plasma, initially self-organized in a solid lattice, was heated and then cooled rapidly by turning laser heating on and off. Particles were tracked using video microscopy, allowing atomistic-scale observation during melting and solidification. During rapid heating, the suspension remained in a solid structure at temperatures above the melting point, demonstrating solid superheating. Hysteresis diagrams did not indicate liquid supercooling in this 2D system.

Strongly coupled plasma is a collection of free charged particles where the Coulomb interaction with nearest neighbors is so strong that particles do not easily move past one another [1]. Plasma can become strongly coupled due to high density as in neutron stars [2], low temperature as in pure ion plasma [3], or high particle charge as in dusty plasma [4]. Dusty plasma is partially ionized gas containing micron-size particles of solid matter. Dusty plasmas have been used in the study of phase transitions [5–9], waves [10], transport [4,11–13], and liquid microstructure [14].

Materials such as water can exist as superheated solid [15] or supercooled liquid [16]. These are, respectively, a solid at temperatures above the melting point [17] and a liquid below the melting point [18]. Observing solid superheating was once thought to be impossible [19], but it is now practical due to new instrumentation for heating [15,20] or fabricating special samples [21,22].

We find that the literature for solid superheating lacks experiments with atomistic-scale observation. Here, the term ''atomistic-scale'' indicates that molecules or their equivalent are imaged or tracked individually. Most solid superheating experiments use external measurements like diffraction in metals [20–22] or optical absorption in ice [15] or electrical measurements for Abrikosov vortices [23]. In contrast to the experimental literature, theory for solid superheating includes simulations that track individual molecules [17]. Experiments with colloidal suspensions include direct imaging of particles in supercooled liquids [24,25], but apparently not superheated solids.

The literature for solid superheating also lacks experiments with strongly coupled plasma. Experiments with strongly coupled plasma have demonstrated solid and liquid [5–8,14] behavior, and recently supercooled liquid as well [9], but not superheated solid.

Liquid supercooling, unlike solid superheating, is easily achieved in many three-dimensional (3D) systems, but it is an open question whether supercooling ever occurs in one-component 2D systems [25]. Experiments are needed to answer this question. Candidate systems for 2D experiments include electrons on a liquid helium surface [26], granular fluids [27], colloids [25], and dusty plasmas [4].

Here, we seek answers to three questions. First, can strongly coupled plasmas exhibit solid superheating? Second, can solid superheating experiments be performed using direct imaging of particles? Third, does our one-component 2D system exhibit liquid supercooling?

We report experiments with a 2D suspension of particles in a dusty plasma, which is a kind of strongly coupled plasma. Highly charged particles, which are polymer microspheres, are immersed in partially ionized argon gas. Electrons and positive ions are collected by a particle, giving it a large negative electric charge. In a plane perpendicular to ion flow, particles interact through a repulsive Yukawa potential $U(r) = Q^2(4\pi\epsilon_0 r)^{-1}\exp(-r/\lambda_D)$ [28].

Our particles experience multiple forces, the largest arising from gravity, electric fields, gas friction, and laser radiation pressure. The apparatus [4] provides a plasma with a sheath above a lower horizontal electrode. This sheath has electric fields that levitate and confine charged particles, so that they are suspended as a single layer. Particles have a diameter 4.83 ± 0.08 μm [29] and mass $m = 8.93 \times 10^{-14}$ kg. To partially ionize 7 mTorr argon gas, we used radio-frequency power at 13.56 MHz, with an amplitude of 97 V peak to peak. Particles experience gas drag with a coefficient of 2.1 s^{-1} [29] when they move.

As in colloidal suspensions, our particles can self-organize in a crystal. Unlike colloids, however, our particles are underdamped, and they can be heated without heating the gas or ions. In our experiment, particle motion was essentially 2D, with negligible out-of-plane displacements and no buckling of the particle layer.

Video microscopy allows imaging this 2D suspension at an atomistic scale, so that we can track particles and measure their individual positions and velocities in each video frame. Viewing from above, we recorded a movie [30] of 5575 frames at 55 frames per second with a total field of view (FOV) of 34.2×25.6 mm^2. We analyzed data in a 30.7×22.2 mm^2 sample region in the center of the FOV, which included about 1000 of the >5000 particles in

the suspension. The particle spacing was characterized by a Wigner-Seitz radius [4] of 0.45 mm. In each frame, we measured positions of particles and tracked their motion. The particle positions were used for three structural indicators, described below. For each video frame, the 2D particle velocities v_i were used to calculate the temperature $T = [\sum_{i=1}^{N} m(v_i - \bar{v})^2/2]/Nk_B$, where N is the number of particles analyzed and $\bar{v}$ is the center-of-mass velocity. This kinetic temperature is different from the temperatures of the other constituents including the neutral gas, electrons, ions, and the polymer material of the particles themselves. Our velocity distribution function contained some non-Maxwellian features, as in [31], including a peak at $v_y^2 = 5$ (mm/s)^2 as in Fig. 4(c) of [31]. Particle velocities were also used in the wave-spectra analysis method [10] to determine the particle charge $Q = -(4360 \pm 440)e$ and the screening length $\lambda_D = (0.65 \pm 0.15)$ mm.

At first, without additional heating, the suspension has the solid structure of a triangular lattice with sixfold symmetry. Because of its extreme softness and the stresses applied by confining electric fields, this solid is never defect-free. Even at the lowest temperatures, it has some defects, arranged in strings defining domain walls [8].

Our laser heating method [4,31] allows adjusting the kinetic temperature of particles by varying the laser power. This does not affect the plasma environment or particle charge, unlike previous methods [5–8]. Random kicks are applied through radiation pressure from a pair of 532-nm laser beams that are rastered across the suspension in a Lissajous pattern with frequencies $f_x = 48.541$ Hz and $f_y = 30$ Hz in a rectangular region slightly larger than the FOV. During laser heating, the suspension is a driven-dissipative system [4]. In steady state, the particle kinetic temperature is determined by a balance of external laser heating and frictional drag cooling from neutral gas. Because of the orientation of the laser beams, the temperature is higher in the x direction [31] by a ratio of 2 during steady heating, and increasing monotonically from 1 to 2 during rapid heating.

To provide conditions favorable for solid superheating or liquid supercooling, we switch the laser on and off abruptly, so that the temperature will change suddenly. In our rapid heating and cooling experiment, the pair of 532-nm laser beams is ramped between 0 and 7 W in 1 or 2 sec, for rapid cooling and heating, respectively. This results in a temperature that changes at a rate >20 000 K/s during rapid heating.

We measure three indicators of microscopic structure in addition to the temperature time series. First, we identify defects and calculate defect area fraction by calculating Voronoi diagrams [7,30]. Second, we measure short-range translational order using the height of the first peak of the pair correlation function $g(r)$ [31], which is larger for solids than for liquids. Third, we measure the short-range orientational order using the bond-angular-order parameter

G_θ [32], which varies from zero for a gas to unity for a perfect crystal. For a solid, G_θ is less than unity if there are defects.

In addition to our measurements with rapid heating and cooling, we also performed slower heating and cooling to measure the melting point, in the range 4600–5600 K. This is consistent with the prediction 4600 ± 1000 K of 2D Yukawa simulations [33] using our measured values of interparticle spacing, Q and λ_D; the error bar arises from uncertainties in Q and λ_D.

Our main results are time series of temperature and the microscopic structure indicators. We applied rapid heating, followed by 55 sec of steady conditions and then rapid cooling. The temperature time series, shown in Fig. 1(a), is marked at six times corresponding to the Voronoi diagrams in Figs. 1(b)–1(g). Time series are presented in Fig. 2 for the structure indicators: defect fraction, $g(r)$ peak value, and G_θ. We combine time series data to yield a hysteresis diagram, Fig. 3. Details are presented next.
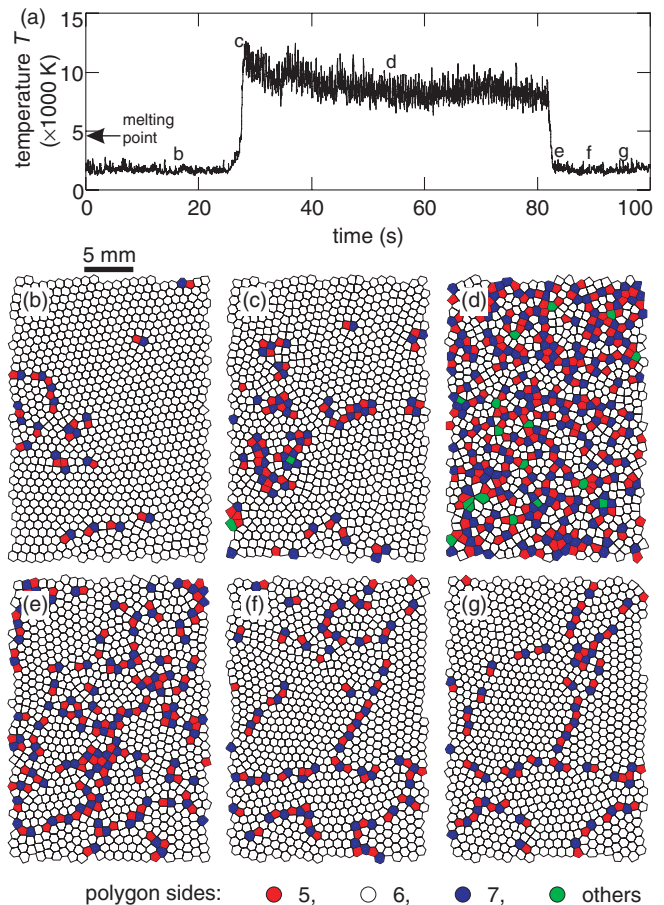

FIG. 1 (color online). (a) Time series of particle kinetic temperature $T(t)$, when laser heating was switched on and then off. Times marked b–g correspond to panels below. (b)–(g) Voronoi diagrams, showing defects in color. Polygons indicate the number of nearest neighbors of a particle.
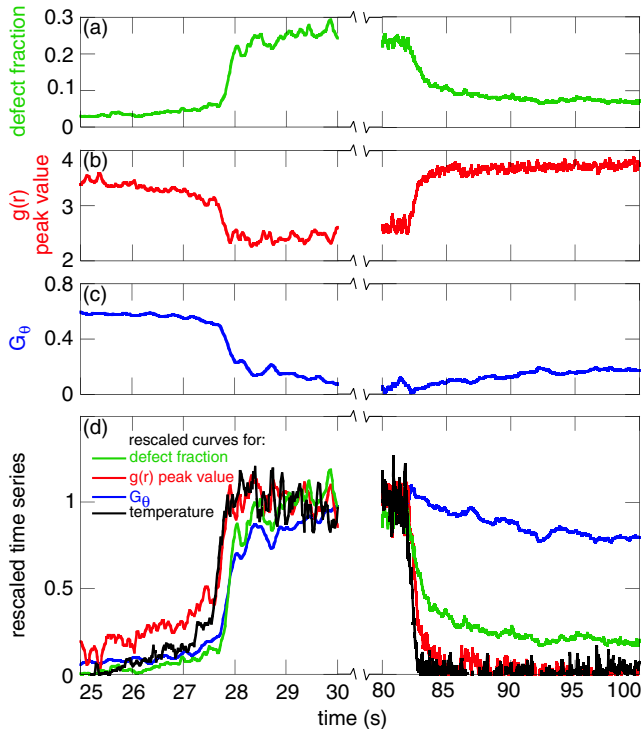
FIG. 2 (color online).   (a) Defect fraction (the area of defective polygons, as a fraction of total area, in Voronoi diagrams as in Fig. 1). (b) Height of the first peak of the pair correlation function $g(r)$. This is an indicator of short-range translational order. (c) G_θ [32], an indicator of short-range orientational order. This can vary from zero for a gas to unity for a perfect crystal. (d) Time series for the three structure indicators and temperature, rescaled to vary from zero (for a solid before heating) to unity (for a liquid during heating). Data are smoothed over three frames.

The sequence of Voronoi diagrams, Figs. 1(b)–1(g), reveals solid superheating. Before heating, Fig. 1(b), the suspension has a solid polycrystalline structure, with domains as large as the sample region shown here. In the most significant panel in this sequence, Fig. 1(c), at $T > 9000$ K near the end of rapid heating, the structure remains a polycrystalline solid, with only a modest increase in defects mostly near the previous defect locations. Since this is a solid structure, while at the same time the temperature is above the melting point, we conclude that it is a superheated solid. Later, in steady heating, Fig. 1(d), the structure is liquid, as indicated by the numerous defects and lack of large crystalline domains. Immediately after rapid cooling, Fig. 1(e), defects have diminished greatly. Five and ten seconds after rapid cooling, Fig. 1(f) and 1(g), respectively, the suspension is again a polycrystalline solid, with crystalline domains separated by string-shaped defect clusters. These crystallites grow bigger by merging neighbors together gradually in a slow recrystallization process [8].

Time series for microscopic structure indicators, Fig. 2, reveal different time scales. In order to compare these time
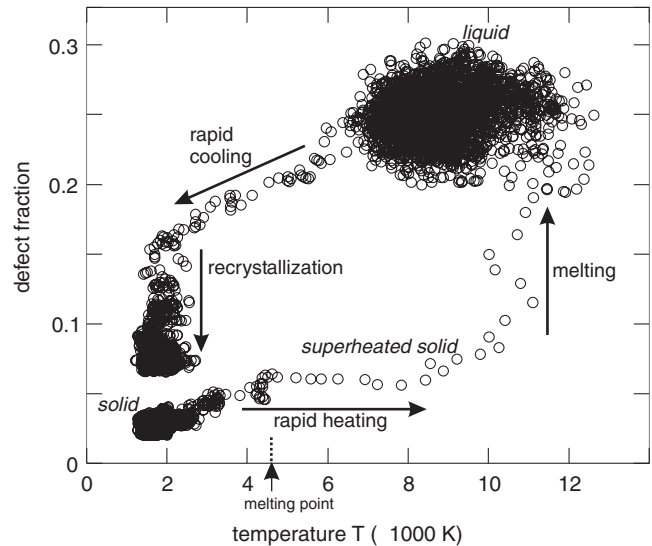

FIG. 3.   Hysteresis diagram made by combining data from Figs. 1 and 2. The time interval between data points is 0.018 sec. Initially, we had a solid, lower left corner. Then rapid heating was applied, causing a temperature increase across the melting point without much change in structure, the lower horizontal line of data points. This is a signature of solid superheating. Next, the superheated solid melted, as shown by the nearly vertical line of data points on the right. The resulting liquid in the upper right corner had a high defect fraction. Later, during rapid cooling, defect fraction dropped dramatically as the temperature declined. Finally, the suspension slowly recrystallized.

scales, we rescaled all four variables in Fig. 2(d) to vary from 0 (before rapid heating) to 1 (during steady heating) using a linear function with a slope and intercept for each variable. During cooling, structure indictors change at different rates: translational order changes fastest and orientational order slowest, consistent with the data of [8]. We also measured the defect fraction, which changed at a rate between the other two. Our experimental method also allows measurements during rapid heating, where we observe a delay in the response of the structure as the temperature increases. This delay is shortest (≤ 0.04 sec) for translational order and longer (≈ 0.2 sec) for defect fraction and orientational order.

Hysteresis diagrams, like Fig. 3, are traditional tools for studying phase transitions [21,34]. Hysteresis arises because structure does not respond immediately to a change of temperature. This can occur either due to a delayed response as in the case of our rapid heating or a gradual response as for our rapid cooling. In previous solid super-heating experiments, the vertical axis was typically from x-ray diffraction [21]. Here we use direct imaging of particles to yield an indicator of microscopic structure for the vertical axis of a hysteresis diagram, Fig. 3. Our hysteresis diagram allows a useful interpretation: a signature of solid superheating or liquid supercooling would be a horizontal row of data points across the melting point. Such a hori-

zontal row would indicate a temperature that has changed without a corresponding change in structure.

Our chief conclusion, an observation of solid superheating, is based on two results. First, Voronoi diagrams compared before and after rapid heating indicate solid superheating, as described above. Second, the hysteresis diagram, Fig. 3, has the signature of solid superheating: a nearly horizontal row of data points, which can be seen near the bottom of the graph.

After the superheated solid is formed, it then melts, as indicated by a proliferation of defects. Because the substance being melted is a superheated solid, the melting occurs without much further temperature increase, yielding a nearly vertical line of data points in Fig. 3. The lifetime of the superheated solid and the duration of the subsequent melting are both about 0.25 sec.

We also conclude that our rapid cooling did not produce a supercooled liquid. The rapid-cooling portion of Fig. 3 lacks the signature of a supercooled liquid. Instead, the defect fraction drops dramatically during the temperature decrease. Additionally, the Voronoi diagrams for rapid cooling, Figs. 1(e)–1(g), lack a liquid structure.

Our observation that we did not form a supercooled liquid might be attributable to the low dimensionality of the experiment. For 3D systems, many examples of materials, including dusty plasma [9], can be quenched to form supercooled liquids or glasses. For 2D systems, however, forming a supercooled liquid or glass seems to be difficult [25]. The role of dimensionality in transitions to a glassy or supercooled state remains an important question [9,35]. A previous 2D experiment addressing this question was performed using colloidal suspensions [25], which have much higher friction than in our suspension.

In addition to our experiment, we also performed a numerical simulation. We found conditions that result in the same signature of transient solid superheating as in the experiment, as we will report in detail elsewhere.

In conclusion, first we have shown that strongly coupled plasmas can exhibit solid superheating. This suggests investigating superheating in other solid strongly coupled plasmas that can melt, like laser-cooled ions [3] and the crust of neutron stars [2]. Second, we have demonstrated an experimental method of studying solid superheating using direct imaging of particles. These two results are apparently the first of their kind. Third, we found a lack of liquid supercooling in our 2D system.

*yan-feng@uiowa.edu

[1] S. Ichimaru, Rev. Mod. Phys. **54,** 1017 (1982).
[2] C. J. Horowitz, D. K. Berry, and E. F. Brown, Phys. Rev. E **75,** 066101 (2007).
[3] M. J. Jensen *et al.*, Phys. Rev. Lett. **94,** 025001 (2005).
[4] B. Liu and J. Goree, Phys. Rev. Lett. **100,** 055003 (2008).
[5] H. M. Thomas and G. E. Morfill, Nature (London) **379,** 806 (1996).
[6] A. Melzer, A. Homann, and A. Piel, Phys. Rev. E **53,** 2757 (1996).
[7] R. A. Quinn and J. Goree, Phys. Rev. E **64,** 051404 (2001).
[8] C. A. Knapek *et al.*, Phys. Rev. Lett. **98,** 015004 (2007).
[9] M. Rubin-Zuzic *et al.*, Nature Phys. **2,** 181 (2006).
[10] S. Nunomura *et al.*, Phys. Rev. Lett. **89,** 035001 (2002).
[11] W. T. Juan and L. I, Phys. Rev. Lett. **80,** 3073 (1998).
[12] V. E. Fortov *et al.*, Phys. Rev. E **75,** 026403 (2007).
[13] V. Nosenko *et al.*, Phys. Rev. Lett. **100,** 025003 (2008).
[14] C. L. Chan and L. I, Phys. Rev. Lett. **98,** 105002 (2007).
[15] H. Iglev *et al.*, Nature (London) **439,** 183 (2006).
[16] R. S. Smith and B. D. Kay, Nature (London) **398,** 788 (1999).
[17] X. M. Bai and M. Li, J. Chem. Phys. **123,** 151102 (2005).
[18] M. D. Ediger, C. A. Angell, and S. R. Nagel, J. Phys. Chem. **100,** 13 200 (1996).
[19] J. G. Dash, Rev. Mod. Phys. **71,** 1737 (1999).
[20] J. W. Herman and H. E. Elsayed-Ali, Phys. Rev. Lett. **69,** 1228 (1992).
[21] L. Gråbæk *et al.*, Phys. Rev. B **45,** 2628 (1992).
[22] L. Zhang *et al.*, Phys. Rev. Lett. **85,** 1484 (2000).
[23] Z. L. Xiao *et al.*, Phys. Rev. Lett. **92,** 227004 (2004).
[24] E. R. Weeks *et al.*, Science **287,** 627 (2000).
[25] H. König *et al.*, Eur. Phys. J. E **18,** 287 (2005).
[26] C. C. Grimes and G. Adams, Phys. Rev. Lett. **42,** 795 (1979).
[27] P. M. Reis, R. A. Ingale, and M. D. Shattuck, Phys. Rev. Lett. **96,** 258001 (2006).
[28] U. Konopka, G. E. Morfill, and L. Ratke, Phys. Rev. Lett. **84,** 891 (2000).
[29] B. Liu *et al.*, Phys. Plasmas **10,** 9 (2003).
[30] See EPAPS Document No. E-PRLTAO-100-033822 for two movies corresponding to the data presented in this Letter. For more information on EPAPS, see http://www.aip.org/pubservs/epaps.html.
[31] V. Nosenko, J. Goree, and A. Piel, Phys. Plasmas **13,** 032106 (2006).
[32] I. V. Schweigert, V. A. Schweigert, and F. M. Peeters, Phys. Rev. Lett. **82,** 5293 (1999).
[33] P. Hartmann *et al.*, Phys. Rev. E **72,** 026409 (2005).
[34] C. J. Olson *et al.*, Phys. Rev. B **67,** 184523 (2003).
[35] M. Bayer *et al.*, Phys. Rev. E **76,** 011508 (2007).